Chemical Engineering Science 64 (2009) 3697 – 3708

Contents lists available at ScienceDirect

Chemical Engineering Science

journal homepage: www.elsevier.com/locate/ces

An experimental study of air–water Taylor flow and mass transfer inside square microchannels

Jun Yue[a,b], Lingai Luo[b,*,1], Yves Gonthier[b], Guangwen Chen[a,*,2], Quan Yuan[a]

[a]Dalian National Laboratory for Clean Energy, Dalian Institute of Chemical Physics, Chinese Academy of Sciences, Dalian 116023, China
[b]Laboratoire Optimisation de la Conception et Ingénierie de l'Environnement (LOCIE), Université de Savoie, Campus Scientifique, Savoie Technolac, 73376 Le Bourget-Du-Lac Cedex, France

ARTICLE INFO

Article history:
Received 23 December 2008
Received in revised form 21 March 2009
Accepted 12 May 2009
Available online 27 May 2009

Keywords:
Microchannel
Taylor flow
Bubble
Hydrodynamics
Mass transfer
Multiphase reactors

ABSTRACT

Flow and mass transfer properties under air–water Taylor flow have been investigated in two square microchannels with hydraulic diameters of 400 and 200 μm. Experimental data on Taylor bubble velocity, pressure drop and liquid side volumetric mass transfer coefficient (k_La) have been presented. It was shown that the measured Taylor bubble velocity in square microchannels could be well interpreted based upon an approximate measurement of the liquid film profile therein. Then, the obtained two-phase frictional pressure drop values in both microchannels were found to be significantly higher than the predictions of the correlation proposed by Kreutzer et al. [2005b. Inertial and interfacial effects on pressure drop of Taylor flow in capillaries. A.I.Ch.E. Journal 51, 2428–2440] when the liquid slug was very short, which can be explained by the inadequacy of their correlation to describe the excess pressure drop caused by the strong inner circulation in such short liquid slugs. An appropriate modification has been made to this correlation in order to improve its applicability in microchannels. Finally, the experimental (k_La) values in the microchannel with hydraulic diameter of 400 μm were found to be in poor agreement with those predicted by the existing correlations proposed for capillaries with diameters of several millimeters. The observed deviation was mainly due to the fact that mass transfer experiments in this microchannel actually corresponded to the case of short film contact time and rather poor mixing between the liquid film and the liquid slug, which was not in accordance with mass transfer assumptions associated with these correlations. A new empirical correlation has been proposed to describe mass transfer data in this microchannel.

1. Introduction

The improvement of multiphase reactor performance via process intensification has been the focus of considerable researches for many years. The newly emerging gas–liquid microreaction technology presents an attractive alterative and has gained increased interests recently among both academic communities and industrial companies (Chen et al., 2008; Ehrfeld et al., 2000; Hessel et al., 2004, 2005a). This technology features in the use of well-defined microchannel structures with diameters in the order of microns to hundreds of microns to perform a variety of gas–liquid operations. The reduction of channel size to micron scale in such microreactors brings numerous advantages that are hardly achievable in their macroscale counterparts. Remarkably high gas–liquid mass transfer rate can be realized primarily because of large surface to volume ratios inherent in microchannels. A better process safety can also be ensured via the excellent thermal management as well as the effective suppression of the flame propagation in microchannels. Thus it is envisaged that plenty of highly exothermic, fast gas–liquid or gas–liquid–solid catalyzed reactions can benefit substantially from the use of gas–liquid microreactors. The available researches have made it clear that gas–liquid microreactors show great potential in a host of applications including gas absorption (TeGrotenhuis et al., 2000; Yue et al., 2007), direct fluorination (Chambers et al., 2001; de Mas et al., 2003; Jähnisch et al., 2000), liquid phase oxidation (Leclerc et al., 2008), three-phase catalytic hydrogenation (Abdallah et al., 2006; Kobayashi et al., 2004; Losey et al., 2001; Yeong et al., 2003), and direct synthesis of hydrogen peroxide (Inoue et al., 2007; Wang et al., 2007). Among these studies, four main types of gas–liquid microreactors have been reported according to two-phase

* Corresponding authors.
E-mail addresses: yuej@dicp.ac.cn (J. Yue), Lingai.Luo@univ-savoie.fr (L. Luo), gwchen@dicp.ac.cn (G. Chen).
[1] Tel.: +33 4 79 75 81 93; fax: +33 4 79 75 81 44.
[2] Tel.: +86 411 84 37 90 31; fax: +86 411 84 37 93 27.

0009-2509/$ - see front matter © 2009 Elsevier Ltd. All rights reserved.
doi:10.1016/j.ces.2009.05.026

contacting principle (Chen et al., 2008; Hessel et al., 2005b), that is, microchannel contactor (or micro bubble column), falling film microreactor, microreactor with phase interface stabilized with physical structures such as meshes and porous plates, and micro packed bed reactor. It seems that microchannel contactor in which gas and liquid flow co-currently inside the same microchannel may be more attractive for future large-scale industrial applications in view of its wide operational range of gas and liquid flow rates, good mass transfer and reaction efficiency under certain gas–liquid two-phase flow patterns, and also relatively easy scale-up process by stacking a multitude of reaction platelets comprising a plurality of microchannels together. The rational design and reliable operation of this type of microreactor require a thorough understanding of fundamental gas–liquid transport process and its interplay with chemical kinetics in microchannels.

Previous studies have indicated that gas–liquid two-phase flow pattern in microchannels mainly includes bubbly, slug, slug–annular, annular, and churn flows, the inner flow details of which are rather different from those observed in large channels (Chung and Kawaji, 2004; Triplett et al., 1999; Yue et al., 2008). This is primarily due to the fact that under most circumstances, surface tension begins to play an important role and laminar flow nature of each phase prevails in microchannels. Among the observed flow patterns, Taylor flow (identified as a sub-regime of slug flow corresponding to the alternative movement of equally long Taylor bubbles and liquid slugs down the channel) is the preferred one for gas–liquid reactions in microchannels, which occurs typically at comparatively low gas flow velocities. In Taylor flow, the liquid slug is separated from each other by the presence of Taylor bubbles and the only means for the communication between two adjacent liquid slugs is through the thin film region between the bubble and the channel wall, thus indicating a significant reduction in axial mixing. For example, recently Trachsel et al. (2005) have measured the residence time distribution (RTD) for single-phase liquid and gas–liquid Taylor flow in microchannel networks by on-site integration of a piezoelectrically activated tracer injection technique. It has been observed that RTD was significantly narrower for Taylor flow case than for laminar flow case at similar conditions. Besides a reduced axial mixing, an improved radial mixing can be also achieved by the recirculation motion inside the liquid slug (Günther et al., 2004; Thulasidas et al., 1997). Moreover, enhanced mass transfer and reaction rates can be offered inside the thin film region (Kreutzer et al., 2001; Vandu et al., 2005). Thus gas–liquid reactions in microchannels will benefit much from the operation under this flow pattern, where the reactions can be further optimized towards conversion and selectivity. From this point of view, Taylor flow has the most priority to be investigated among all possible flow patterns present in microchannels.

Although numerous investigations on transport and reaction properties of Taylor flow in minichannels or capillaries with diameters on the orders of millimeters have been performed during the past several ten years (Angeli and Gavriilidis, 2008; Kreutzer et al., 2005a), the relevant studies further down to microchannels (especially with non-circular channel shapes) have not been frequently seen up to now. Thus it is still not clear whether Taylor flow in microchannels presents novel properties when compared to large capillaries. Accordingly, the extrapolation of the available correlations or models proposed for the latter case might be questionable in microchannels, which requires further experimental validation.

In view of the above summary, this paper serves to provide further insights into Taylor flow in square microchannels, where the bubble motion, pressure drop and mass transfer characteristics are mainly concerned. First, experiments on air–water Taylor flow have been performed in two microchannel contactors which consist of Y-shaped square microchannels with hydraulic diameters of 400 and 200 μm, respectively. Taylor bubble velocity, lengths of Taylor bubbles and liquid slugs, two-phase frictional pressure drop data were measured in both microchannels. For the 400 μm hydraulic diameter microchannel, liquid side volumetric mass transfer coefficient was also determined simultaneously under typical operational conditions. Then, based on the obtained data, the applicability of the available correlations from the open literature for describing flow and mass transfer properties of Taylor flow was further examined in the present microchannels. The possible reasons responsible for the observed deviation between the predictions and the experimental results were discussed and some appropriate modifications were also suggested.

2. Experimental apparatus and procedure

2.1. Microchannel contactor specification

The small channel dimension in gas–liquid microreactors usually makes it difficult to perform a direct measurement of fluid pressure or concentration inside the microchannel. Thus in the present work, an indirect measurement approach was used in order to derive pressure drop and mass transfer data in the interested microchannel test section. In detail, two different types of single microchannel contactors have been tested, as described below.

The first type of single microchannel contactor mainly consists of a Y-shaped square microchannel structure (with hydraulic diameter of 400 or 200 μm, respectively) fabricated on the polymethyl methacrylate (PMMA) substrate by using a precision micromilling machine, as schematically illustrated in Fig. 1(a). The microchannel plate was capped with a piece of transparent adhesive and then compressed against another smooth PMMA plate using screw

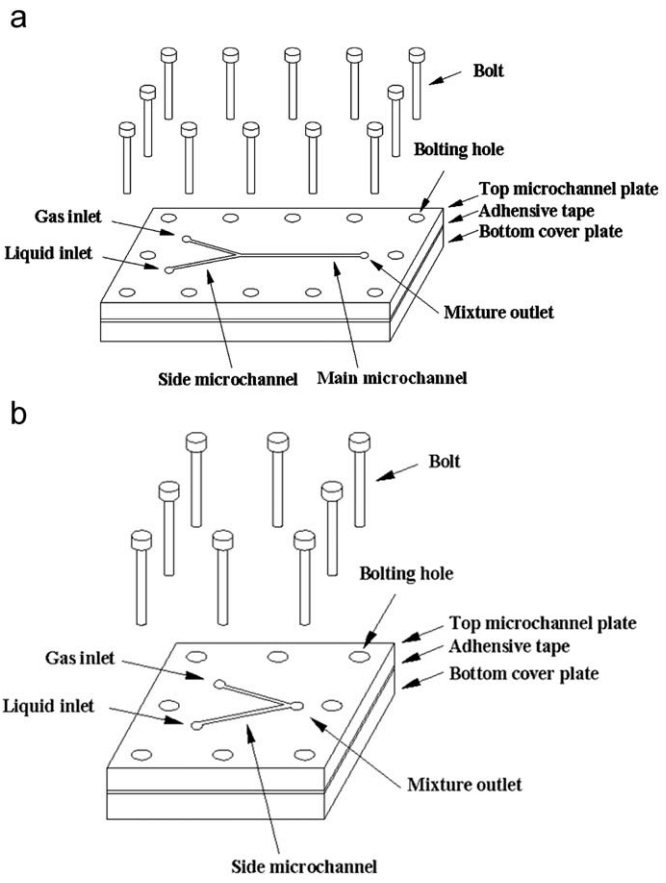

Fig. 1. Schematic representation of microchannel contactors: (a) SMC I and (b) SMC II.

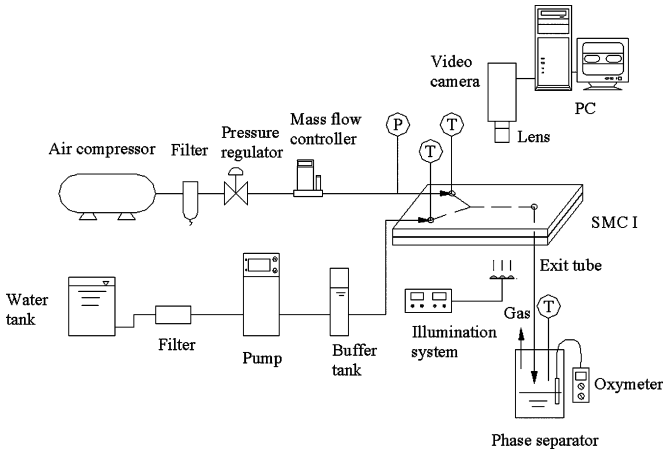

Fig. 2. Experimental rig for flow and mass transfer study under air–water Taylor flow in microchannel contactors.

fittings through the punched holes on the peripheries of both plates in order to form a closed microchannel section for fluid passage. Gas and liquid are introduced into the contactor through the connectors machined on the backside of the microchannel plate and flow along two respective side microchannels (2.53 cm long) prior to their contact in the main microchannel (4.8 cm long). This type of contactor will be referred to as SMC I hereafter.

The second type of single microchannel contactor (termed as SMC II) was employed for the purpose of measuring equivalent pressure drop or mass transfer contributions in the outlet zone of SMC I, as shown in Fig. 1(b). It adopted the same fabrication and sealing methods as those for SMC I. From Figs. 1(a) and (b), it is seen that the only difference between the two types of contactors lies in the fact that in SMC II two side microchannels are directly fed with the outlet plenum while the other channel dimensions remain identical to SMC I.

2.2. Experimental setup

We first carried out air–water Taylor flow experiments in SMC I with $d_h = 400\,\mu m$ under a variety of gas and liquid flow rates, where mass transfer measurements were also performed simultaneously under most circumstances. Fig. 2 is a schematic of the experimental rig. Air source was provided via the air compressor. After flowing through a filter to remove possible contaminations, the pressure of air was adjusted by a pressure regulating valve. Prescribed flow rate of air was designated by a mass flow controller covering a flow range of 0–10 SCCM (Aalborg, Model GFC 17). Then air stream was directly fed into one side microchannel of the contactor that was placed horizontally and the static pressure in the gas feeding line was measured by a pressure transducer with a range of 0–100 kPa (Kobold, Model SEN-3276 B025). Liquid phase used was deionized water that was stored in a tank. Before each run, nitrogen was employed to strip possible dissolved oxygen out. An electronic metering pump with a range of 0–40 ml/min (Eldex, Model 2HM) was then used to draw certain amount of water from the tank into another side microchannel of the contactor. A buffer tank was used here with the aim of dampening the pulsation of liquid flow rate provided by the pump. To avoid possible absorption in the buffer tank, it was purged with nitrogen at regular intervals. The accurate liquid flow rate under each run was measured by weighing method. The flow rates of gas and liquid were selected such that flow pattern in the main microchannel turned to be Taylor flow. After passing the main microchannel, two-phase mixture was directed into an open phase separator via a vertically downward pipe with an inner diameter of 4 mm. Three thermocouples (K-type) were located in the inlet ports and the separator to measure the corresponding temperatures. When the volume of the exit water collected in the separator reached a certain value (about 30 ml), the dissolved oxygen content therein was analyzed by an oxygen electrode (Laboratoires Merck-Clevenot, Model OXY85 T). A similar analysis was also performed for the inlet water inside the tank during each run. All experiments were conducted under ambient conditions (0.1 MPa, 24–26 °C).

For SMC I with $d_h = 200\,\mu m$, no mass transfer measurement was performed in view of the fact that the time to collect enough amounts of the exit water as required by the present analysis method was extremely long (typically > 20 min). In such long period, a stable operation was found to be difficult. Thus for this contactor, only two-phase flow experiments were conducted by using the test facilities shown in Fig. 2.

During experiments with SMC I with $d_h = 400$ and $200\,\mu m$, a high speed video camera (Photron Fastcam PCI R2) placed above the contactor was employed to record the images of Taylor flow in the main microchannel. This camera has the recording rate up to 250 frames/s at full resolution of 512×480 pixels and up to 1000 frames/s at reduced resolution. The camera was further equipped with a megapixel lens (Pentax C2514-M) as well as a set of extension tubes in order to magnify a section of the microchannel under investigation. The light needed for the illumination of the microchannel was provided by a self-made LED lamp which was placed beneath the microchannel. The recorded large amounts of images were first stored in the PCI board's memory and were then stored in the hard disk of a computer for later analysis.

To estimate the equivalent pressure drop or mass transfer contribution in the outlet zone of SMC I, experiments were also conducted in the corresponding SMC II under the same volumetric flow rates of gas and liquid as those for SMC I. The other experimental details remained unchanged.

2.3. Image analysis

During experiments with SMC I, Taylor bubble velocity in the middle section of the main microchannel (at a distance of 2.4 cm from the entrance) was first determined from the images captured by the high speed video camera. If the frame speed was set to be sufficiently high (typically 500 frames/s in this study), the same bubble could reside in two successive images. The distance traveled by the bubble during this short period could be measured easily from the variation of the pixel values in the two images. The bubble velocity was then calculated by dividing the distance it traveled by the time interval between the two images. Under each operational condition, a sequence of at least 20 images were analyzed and the resulted bubble velocity data were averaged together to obtain the final value. It was found that the obtained bubble velocity in these images remained nearly constant with the standard deviation lower than 3%.

Lengths of Taylor bubbles and liquid slugs in the middle section of both microchannels were also measured from the corresponding images. A stable bubble or liquid slug length was observed under a fixed operation condition, where the standard deviations in the measured lengths were found to be both lower than 5%.

3. Results and discussion

3.1. Taylor bubble velocity

During Taylor flow through microchannels, a thin film region usually presents between the body of Taylor bubble and the channel wall. When both gas and liquid are assumed to be incompressible, Griffith and Wallis (1961) have shown that the mean velocity in

the liquid slug U_{slug} can be calculated from the volume continuity equation as

$$U_{slug} = \frac{Q_G + Q_L}{A_{mc}} \tag{1}$$

where Q_G and Q_L are the volumetric flow rates of gas and liquid and A_{mc} the cross-sectional area of the microchannel. Eq. (1) can be further reduced to

$$U_{slug} = j_G + j_L \tag{2}$$

where j_G and j_L refer to the superficial gas and liquid velocities, respectively.

Also the volume continuity equation will lead to

$$Q_G + Q_L = U_B A_B + U_{film} A_{film} \tag{3}$$

Here U_B and U_{film} are the velocities of Taylor bubble and the liquid film, A_B and A_{film} are the cross-sectional areas of Taylor bubble and the liquid film. Then it is obvious that

$$A_{mc} = A_B + A_{film} \tag{4}$$

From Eqs. (1)–(4), Taylor bubble velocity can be expressed as

$$U_B = \frac{U_{slug} A_{mc} - U_{film} A_{film}}{A_{mc} - A_{film}} \tag{5}$$

Thus it is clear that Taylor bubble velocity in microchannels depends crucially on the flow condition of the liquid film (i.e., its average velocity and cross-sectional fraction). When the microchannel is placed horizontally, the gravity effect on the flow of the liquid film vanishes. For air–water Taylor flow under this orientation, it is usually reasonable to assume that the liquid film is nearly at rest especially at comparatively low capillary numbers $Ca = \mu U_B/\sigma$ (i.e., $U_{film} \approx 0$), as revealed by the simulation of Kreutzer et al. (2005b). Then, it is obtained from Eq. (5) that

$$\frac{U_B}{U_{slug}} = \frac{1}{1 - \frac{A_{film}}{A_{mc}}} \tag{6}$$

In this study, Taylor bubble velocity in the middle section of two square microchannels with $d_h = 400$ and 200 μm was determined from the images captured by the high speed video camera, where the superficial velocities ranged from 0.02–1.2 m/s for the gas and 0.33–1.0 m/s for the liquid in the experiments. Fig. 3 depicts the measured U_B as a function of U_{slug} for the two microchannels. Here in order to compensate for the gas compressibility effect, U_{slug} was calculated from Eq. (2) in which j_G was evaluated by using the gas density based on the average pressure between the entrance and outlet of the microchannel (for this system, the amount of gas absorption was insignificant as compared to the gas flow rate so that a constant gas mass flow rate can be assumed throughout the whole microchannel). For other parts in this paper, j_G was derived in the same way. It can be observed in Fig. 3 that the air bubble in both microchannels moves slightly faster than the liquid slug, which is more significant at relatively high U_{slug}. From the above simplified analysis, it is concluded that this phenomenon is mainly resulting from the presence of a nearly stagnant film section surrounding the body of the bubble.

To provide a more reliable explanation of Taylor bubble velocity observed in the current microchannels, it is essential to know the cross-sectional fraction occupied by the liquid film, A_{film}/A_{mc}, as Eq. (6) suggests. This requires that the thickness distribution of the liquid film surrounding the body of the bubble be well understood. It is noticed from the literature that many experimental and theoretical correlations on liquid film thickness are available for horizontal Taylor flow in circular capillaries and even in microchannels (Aussillous and Quéré, 2000; Bretherton, 1961; Chen, 1986; Fairbrother and Stubbs, 1935; Taylor, 1961), whereas only a few relevant studies have been devoted to their square counterparts (Fries et al., 2008; Kolb and Cerro, 1991; Wong et al., 1995a,b). This is primarily due to the fact that the presence of four sharp corners in a square microchannel will have a complicated impact on the bubble shape as well as the liquid film distribution along the channel wall. In detail, the body of Taylor bubble in a circular microchannel can be treated as an ideal axisymmetric cylinder surrounded by the liquid film with even thickness (see Fig. 4(a)). However, for square microchannels as described in this study, the bubble symmetry turns to be firstly dependent on *Ca* (Kolb and Cerro, 1991). At low *Ca*, the bubble is non-axisymmetric (see Fig. 4(b)), which means that the bubble surface is flat near the center of the channel wall and is cylindrical in four corners. In other words, the liquid film is curved in the corner and becomes flat far away from the corner. A transition in bubble symmetry is initiated at higher *Ca*, where the whole bubble body becomes cylindrical (see Fig. 4(c)). The transitional *Ca* was experimentally observed by Kolb and Cerro (1991) to be about 0.1 for upward air–silicone oil flow in a square capillary with $d_h = 2$ mm. Later Thulasidas et al. (1995) determined the transitional point with more accuracy, to take place at $Ca \approx 0.04$. In both cases, the distribution of the film thickness in square microchannels is uneven around the bubble. That is, the film

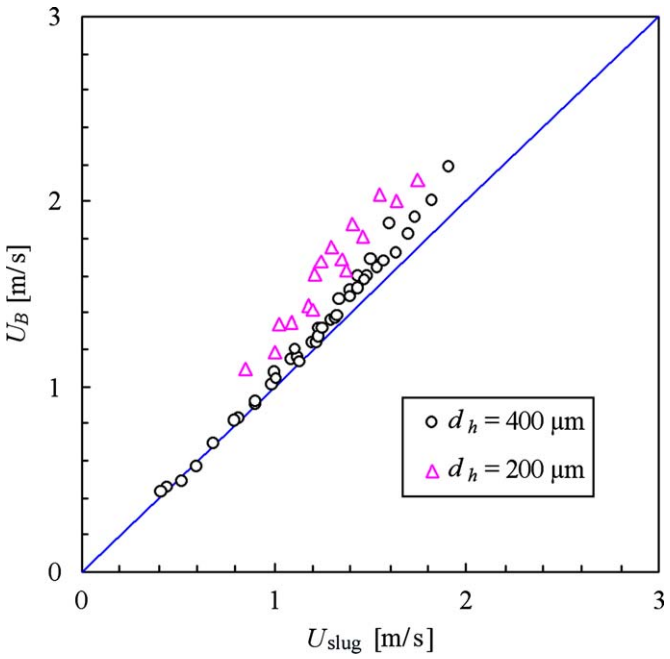

Fig. 3. Taylor bubble velocity versus the mean velocity in the liquid slug in square microchannels.

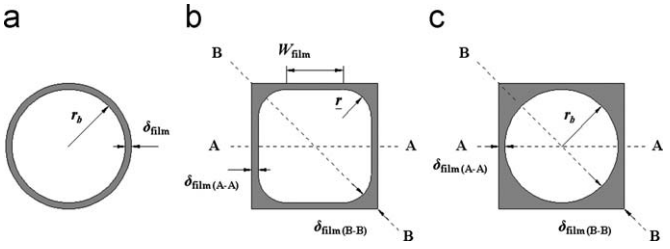

Fig. 4. Liquid film shape in different microchannel geometries: (a) circular, axisymmetric bubble, (b) square, non-axisymmetric bubble, and (c) square, axisymmetric bubble.

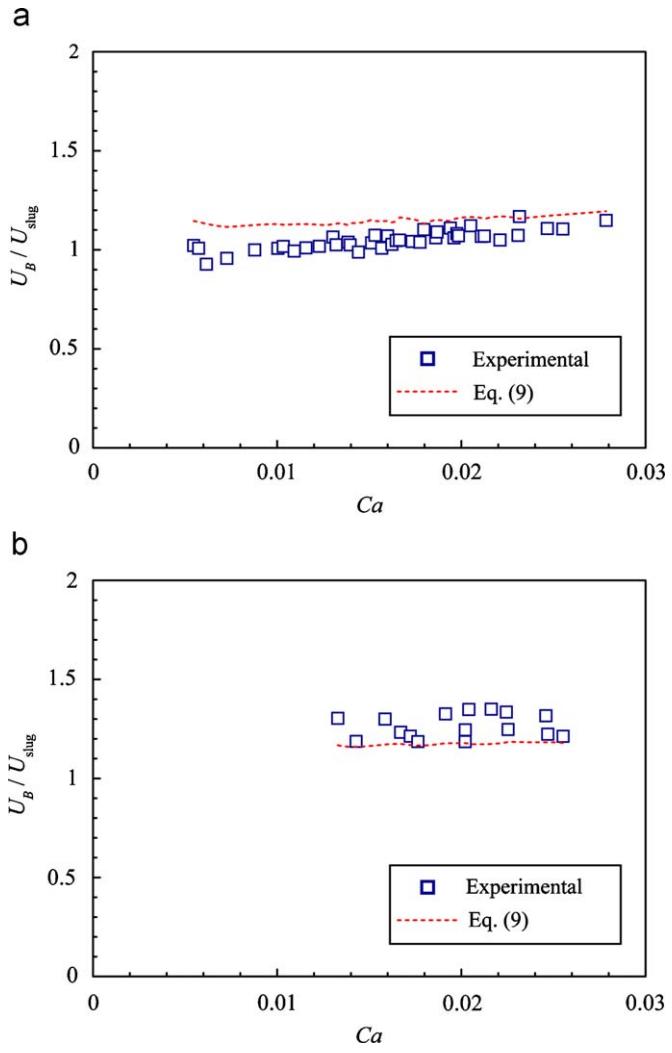

Fig. 5. Velocity ratio between Taylor bubble and the liquid slug as a function of *Ca* in square microchannels: (a) $d_h = 400\,\mu m$ and (b) $d_h = 200\,\mu m$.

thickness in the diagonal plane *B–B*, $\delta_{film\ (B-B)}$, is always larger than that in the axial plane *A–A*, $\delta_{film\ (A-A)}$. Since our experiments were performed under the condition of $Ca < 0.04$ (see Fig. 5), it is thought that the liquid film configuration in the investigated microchannels is alike to that shown in Fig. 4(b). This assumption is further corroborated by the experimental data shown in Fig. 5, as can be seen that the obtained U_B/U_{slug} is generally less than 1.3. While for the liquid film configuration depicted in Fig. 4(c), the liquid film occupies more than 21.5% of the channel cross-section as the bubble diameter should be less than the channel width or height. Thus in the latter case, the bubble should move at a velocity faster than about 1.3 times U_{slug} according to Eq. (6).

For the liquid film configuration in Fig. 4(b), it is easy to show that

$$A_{film} = 4\delta_{film\ (A-A)}\left(d_h - \delta_{film\ (A-A)}\right) + 4\left(1 - \frac{\pi}{4}\right)\underline{r}^2 \tag{7}$$

$$\underline{r} = \frac{d_h}{2} - \frac{W_{film}}{2} - \delta_{film\ (A-A)} \tag{8}$$

Note that in the above two equations the value of d_h is equal to the channel width or height since here a square geometry is dealt with.

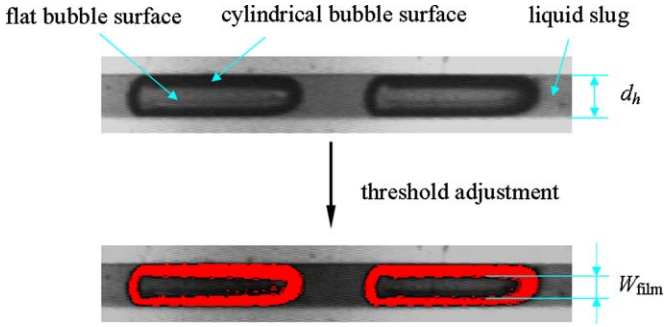

Fig. 6. Scheme for the determination of W_{film} in square microchannels ($d_h = 400\,\mu m$, $j_G = 0.65$ m/s, $j_L = 0.36$ m/s).

Then we can further rewrite Eq. (6) as

$$\frac{U_B}{U_{slug}} = \frac{1}{\left(1 - 2\frac{\delta_{film\ (A-A)}}{d_h}\right)^2 - \left(1 - \frac{\pi}{4}\right)\left(1 - 2\frac{\delta_{film\ (A-A)}}{d_h} - \frac{W_{film}}{d_h}\right)^2} \tag{9}$$

Thus it is seen that the obtained U_B/U_{slug} data should be interpreted based on a reliable estimation of the values of $\delta_{film\ (A-A)}$ and W_{film}. With the captured Taylor flow images, we first performed an approximate measurement of W_{film} in both microchannels, as illustrated in Fig. 6. By using a shareware software ImageJ (version 1.42a, National Institute of Health, USA), the brightness values of the pixels in the acquired black and white images were analyzed. Since there exists a flat gas–liquid interface near the center of the microchannel cross-section and the interface around the corner is cylindrical, the body of the bubble shown in the captured images turns to be very light in the center region and to be very dark in the corner region. The boundary between the two regions can be approximately identified via a brightness threshold adjustment. As a result, the whole bubble surface in the image was marked as red except the flat region. Then the width of this unmarked region could be determined as W_{film}, as shown in Fig. 6. Meanwhile, it is also observed from this figure that the liquid film surrounding the bubble in the axial plane is extremely thin and thus $\delta_{film\ (A-A)}$ cannot be measured directly. The existing studies have made it clear that when *Ca* is less than 0.04, the film thickness in this plane virtually varies little and a constant value of about 0.02 can be assumed for $\delta_{film\ (A-A)}/d_h$ (Fries et al., 2008; Kolb and Cerro, 1991). Consequently, the same assumption is adopted in our analysis as well. With thus obtained W_{film} and $\delta_{film\ (A-A)}$ data, the value of U_B/U_{slug} was further estimated according to Eq. (9) and its comparison with our experimental observation is further plotted in Fig. 5. It can be seen that the experimental data in both microchannels agree well with the predictions of Eq. (9). From Fig. 5 it is also observed that the bubble tends to move more quickly than the liquid slug when *Ca* is increased. To explain this, the measured W_{film}/d_h is plotted as a function of *Ca* in Fig. 7. It is clear that the width of the flat film region decreases with increasing *Ca*, implying the thickening of the liquid film in the diagonal plane. Thus it is suggested that the liquid film will occupy more fraction of the microchannel cross-section at increased *Ca*, leading to comparatively high value of U_B/U_{slug}.

3.2. Pressure drop characteristics

For engineering calculations, two-phase pressure drop correlations solely based on input parameters are more favorable. Both the homogeneous and separated flow models serve this purpose (Wallis, 1969), where the flow pattern information inside channels is not a necessity. However, it seems unconvincing to apply these models

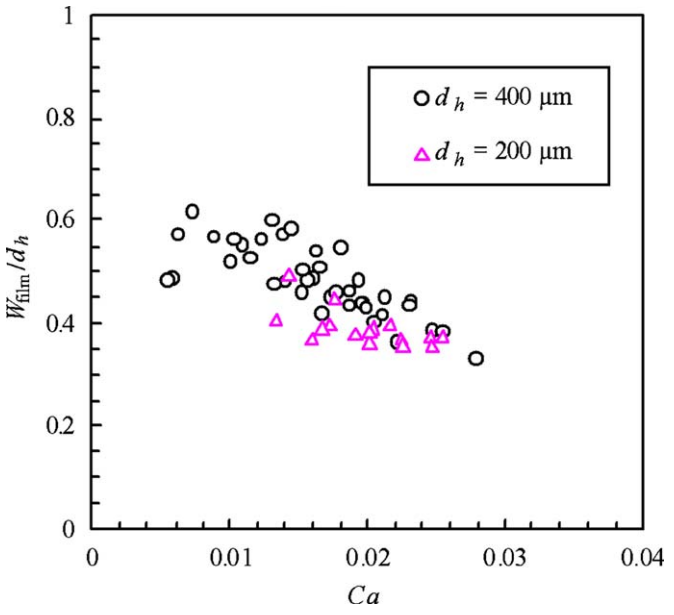

Fig. 7. Measured W_{film}/d_h as a function of Ca in square microchannels.

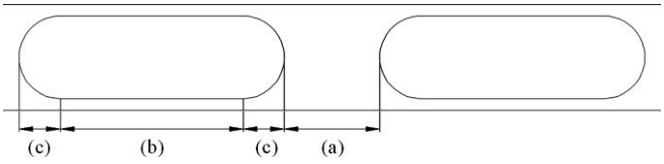

Fig. 8. Diagram of different pressure drop regions in a unit cell of Taylor flow: (a) liquid slug, (b) liquid film, and (c) bubble caps.

directly to Taylor flow in microchannels (Liu et al., 2005; Yue et al., 2008). Actually, Taylor flow is operated under transient conditions due to the discontinuous motion of gas and the alternative expose of the channel wall to the liquid slug and the liquid film. Consequently, this flow pattern can be regarded as neither a homogeneous flow nor a separated flow. This implies that specific details inside Taylor flow should be fully considered in the search of suitable pressure drop correlations.

3.2.1. Pressure drop model

In fact, if we view Taylor flow as a quasi-steady process, two-phase frictional pressure drop in a unit cell (one bubble plus one liquid slug), $\Delta P_{F,uc}$, can be decomposed into three components according to the classification shown in Fig. 8 (Dulkler and Hubbard, 1975; Garimella et al., 2002; Kreutzer et al., 2005b): (1) frictional loss in the liquid slug, $\Delta P_{slug,uc}$; (2) frictional loss in the liquid film, $\Delta P_{film,uc}$; and (3) pressure drop over the front and the rear bubble caps, $\Delta P_{cap,uc}$. Thus it is obtained that

$$\Delta P_{F,\,uc} = \Delta P_{slug,\,uc} + \Delta P_{film,\,uc} + \Delta P_{cap,\,uc} \tag{10}$$

Then two-phase frictional pressure drop gradient in Taylor flow can be deduced as

$$\left(\frac{\Delta P_F}{\Delta L}\right)_{TP} = \frac{1}{L_B + L_S}(\Delta P_{slug,\,uc} + \Delta P_{film,\,uc} + \Delta P_{cap,\,uc}) \tag{11}$$

where L_B and L_S are lengths of Taylor bubbles and liquid slugs. It is seen from Eq. (11) that the specific knowledge on each pressure drop component in a unit cell is required for the estimation of pressure drop in Taylor flow. Below is a detailed description based on the available publications.

Under typical operational conditions relevant to Taylor flow in microchannels, both gas and liquid flows are in laminar regime. As conjectured by Taylor (1961) and then experimentally observed by many authors (Cox, 1964; Günther et al., 2004; Thulasidas et al., 1997), the flow in the liquid slug at Ca lower than about 0.5 is characterized by recirculation patterns near the bubble caps if viewed from a coordinate system moving with the bubble. But if the liquid slug is not very short, the velocity profile will quickly become fully developed (Thulasidas et al., 1997; van Baten and Krishna, 2004). Then for a first approximation, $\Delta P_{slug,\,uc}$ can be assumed as the sum of the extra pressure drop caused by the inner recirculation, $\Delta P_{recirculation,\,uc}$, and the laminar flow pressure drop under fully developed condition in the liquid slug, that is,

$$\Delta P_{slug,\,uc} = \frac{C}{Re_{slug}}\frac{L_S \rho_L U_{slug}^2}{2d_h} + \Delta P_{recirculation,\,uc} \tag{12}$$

where C is laminar friction constant and liquid slug Reynolds number Re_{slug} is defined as $Re_{slug} = d_h U_{slug}\rho_L/\mu_L$.

For horizontal Taylor flow in microchannels, it is usually reasonable to assume that the liquid film is nearly at rest (Kreutzer et al., 2005b). Thus $\Delta P_{film,\,uc}$ is negligible as compared to $\Delta P_{slug,\,uc}$. However, this assumption may be only applicable to situations in which pure liquid is used. When a certain amount of surfactant is involved, Marangoni effect seems to have an important role to play. As an example, the experiments of Fuerstman et al. (2007) showed that the flow of liquid containing intermediate concentrations of surfactant through four corners of rectangular microchannels was not negligible and therefore the frictional loss in the liquid film region contributed greatly to the total two-phase frictional pressure drop.

The pressure drop over the bubble caps in circular capillaries under the condition of sufficiently small non-zero Ca was shown theoretically by Bretherton (1961) to be

$$\Delta P_{cap,\,uc} = 7.16(3Ca)^{2/3}\frac{\sigma}{d_h} \tag{13}$$

Later Wong et al. (1995b) found that the pressure drop over the bubble caps in square capillaries is about one third that in circular ones of the same d_h. Both works did not consider the inertial effect, which is usually not negligible in practical operations. For example, Re_{slug} in the present study was found to be in the range of 180–830 and 195–405 in two microchannels with $d_h = 400$ and 200 μm, respectively. As a result, the influence of inertia on the bubble shape can be easily seen. At higher values of Re_{slug}, the bubble front cap becomes more elongated and the rear cap turns to be more flattened. Consequently, an alternative expression to Eq. (13) should be developed in order to account for the significant inertial effect occurred in the real circumstances.

Based on the above description, two-phase frictional pressure drop gradient in Taylor flow through a microchannel can be further written as

$$\left(\frac{\Delta P_F}{\Delta L}\right)_{TP} = \frac{1}{L_B + L_S}\left(\frac{C}{Re_{slug}}\frac{L_S \rho_L U_{slug}^2}{2d_h} + \Delta P_{recirculation,\,uc} + \Delta P_{cap,\,uc}\right) \tag{14}$$

Here the explicit expressions for $\Delta P_{recirculation,\,uc}$ and $\Delta P_{cap,\,uc}$ are still not clear. Recently, Kreutzer et al. (2005b) experimentally investigated pressure drop characteristics of Taylor flow (air–water, air–decane, and air–tetradecane) in a 2.3 mm diameter capillary and conducted CFD simulation to verify their experimental findings. They suggested that the overall contribution of $\Delta P_{recirculation,\,uc}$ and $\Delta P_{cap,\,uc}$ could be estimated from the results of CFD simulation. In detail, a function ξ was designated to describe their contribution

and then Eq. (14) is further rearranged to

$$f_{\text{slug}} = \frac{C}{Re_{\text{slug}}}(1+\xi) \tag{15}$$

where

$$\xi = a\left(\frac{L_S}{d_h}\right)^{-1}\left(\frac{\rho_L d_h \sigma}{\mu_L^2}\right)^{1/3} \tag{16}$$

and f_{slug} is the apparent slug friction factor defined as

$$f_{\text{slug}} = \frac{\left(\frac{\Delta P_F}{\Delta L}\right)_{TP} d_h}{\frac{\rho_L U_{\text{slug}}^2}{2}} \frac{L_B + L_S}{L_S} \tag{17}$$

The coefficient a in Eq. (16) was determined numerically to be 0.07, however, the experimental findings supported a higher value of 0.17. They claimed that this large difference might be caused by Marangoni effect of small amounts of impurities, which was not considered in the simulations, but was likely to be present in the experiments.

In this work, pressure drop data of air–water Taylor flow were collected in two square microchannels with $d_h = 400$ and 200 μm. A comparison between the obtained results and the predictions of the Kreutzer correlation (i.e., Eq. (15)) will be performed in the following section, based on which some more light will be shed on pressure drop characteristics of Taylor flow in microchannels.

3.2.2. Experimental verification

In the present experimental setup, two-phase total pressure drop ΔP_T in the main microchannel of SMC I was derived indirectly by a comparison with the results from reference experiments with the corresponding SMC II. Further information concerning pressure data reduction method can be found in our previous paper (Yue et al., 2008). Thus it is obtained that

$$\Delta P_T = P_{\text{in, SMCI}} - P_{\text{in, SMCII}} \tag{18}$$

Here $P_{\text{in, SMCI}}$ and $P_{\text{in, SMCII}}$ denote the inlet pressures measured in the gas feeding line during experiments with SMCs I and II, respectively.

Then two-phase frictional pressure drop gradient can be derived as

$$\left(\frac{\Delta P_F}{\Delta L}\right)_{TP} = \frac{\Delta P_T - \Delta P_A}{\Delta L} \tag{19}$$

where ΔP_A is two-phase acceleration pressure drop given by

$$\Delta P_A = G^2\left[\left(\frac{x^2}{\rho_G \varepsilon_G} + \frac{(1-x)^2}{(1-\varepsilon_G)\rho_L}\right)_1 - \left(\frac{x^2}{\rho_G \varepsilon_G} + \frac{(1-x)^2}{(1-\varepsilon_G)\rho_L}\right)_0\right] \tag{20}$$

The gas hold up data at the microchannel entrance and outlet needed in Eq. (20) were estimated approximately by using the Armand correlation. That is,

$$\varepsilon_G = 0.833\beta \tag{21}$$

where $\beta = j_G/(j_G + j_L)$. This empirical correlation has been shown by many authors to well represent gas hold up data measured during Taylor flow of air–water like fluid pairs in microchannels under relatively wide operational conditions (Serizawa et al., 2002; Warnier et al., 2008; Yue et al., 2008; Zhao and Bi, 2001).

Finally, the product of the apparent slug friction factor and liquid slug Reynolds number, $(fRe)_{\text{slug}}$, can be measured from the experiments as

$$(fRe)_{\text{slug}} = \frac{2\left(\frac{\Delta P_F}{\Delta L}\right)_{TP} d_h^2}{U_{\text{slug}}\mu_L} \frac{L_B + L_S}{L_S} \tag{22}$$

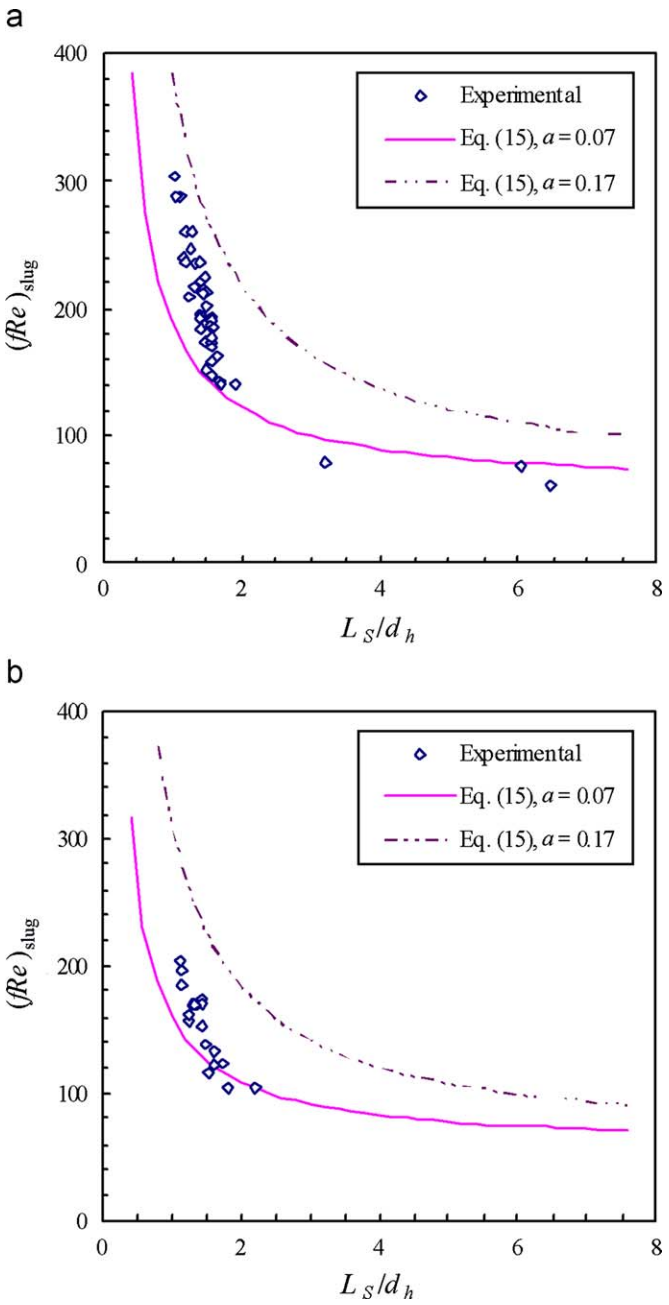

Fig. 9. $(fRe)_{\text{slug}}$ as a function of L_S/d_h in square microchannels: (a) $d_h = 400$ μm and (b) $d_h = 200$ μm.

Fig. 9 plots the measured $(fRe)_{\text{slug}}$ as a function of L_S/d_h in two microchannels and its comparison with the prediction of the Kreutzer correlation, Eq. (15). In view of square microchannel cross-section investigated in this study, C value in Eq. (15) was set as 56.9 (Shah and London, 1978). From Fig. 9 it is first seen that at large values of L_S/d_h, the obtained $(fRe)_{\text{slug}}$ data in both microchannels generally agree well with those predicted by Eq. (15), provided that the numerically derived value of 0.07 is assigned for the coefficient a. Nevertheless, it is also noticed that Eq. (15) with $a = 0.07$ significantly underpredicts the experimental $(fRe)_{\text{slug}}$ values when L_S/d_h is lower than about 1.5. Recall that in the simulation of Kreutzer et al. (2005b), a boundary condition of fully developed laminar flow profile was explicitly imposed on both ends of two half liquid slugs surrounding the same bubble. This condition is usually satisfied so

long as the liquid slug is not very short (Thulasidas et al., 1997; van Baten and Krishna, 2004). For example, Thulasidas et al. (1997) determined velocity distributions in the liquid slug inside capillaries of circular and square cross-section with $d_h = 2$ mm via particle imaging velocimetry (PIV). Their results revealed that if the liquid slug was longer than 1.5 times the capillary diameter, at a short distance from the bubble caps streamlines were straight, indicating a fully developed laminar flow in the liquid slug. Thus Eq. (15) is thought to be capable of describing pressure drop of Taylor flow containing comparatively long liquid slugs. But it can be seen from Fig. 9 that liquid slug lengths in both microchannels were rather short in the majority of our experiments (normally ranging from $1d_h$ to $1.5d_h$). In such short liquid slugs, Thulasidas et al. (1997) have found that streamlines were everywhere curved, indicating that a fully developed laminar flow velocity profile could not be recovered and that the whole liquid slug region was actually dominated by a strong recirculation pattern. Thus it is expected that the simulation of Kreutzer et al. (2005b) tends to underpredict the contribution of the extra pressure drop caused by the inner recirculation, $\Delta P_{\text{recirculation, }uc}$, to a large extent when the liquid slug is rather short. As a result, it has been observed in the present study that the measured $(fRe)_{\text{slug}}$ value is much higher than the prediction of Eq. (15) with $a = 0.07$ when the liquid slug is shorter than 1.5 times the microchannel hydraulic diameter.

From Fig. 9 it is further observed that if the experimentally derived value of 0.17 in the work of Kreutzer et al. (2005b) is assigned for the coefficient a in Eq. (15), this equation will yield much higher $(fRe)_{\text{slug}}$ values than the measured ones in both microchannels. Kreutzer et al. (2005b) argued that the better fit of Eq. (15) with $a = 0.17$ to their experimental data was likely because of Marangoni effect present in their experiments. Thus the comparison shown in Fig. 9 suggests that Marangoni effect in our experiments is unimportant, which might be explained based on the following considerations: (i) although water used in this study probably contained traces of impurities, the build-up of a significant concentration gradient of these surface-active contaminants along gas–liquid interface seemed not to occur in view of the fact that the residence time of Taylor bubbles inside the microchannel was rather short (ranging from 21 to 112 ms) (Schulze and Schlünder, 1985; Vasconcelos et al., 2002) and (ii) Marangoni effect is most significant at low Ca (typically $< 10^{-3}$). At large Ca, the bubble velocity becomes so large that Marangoni convection along gas–liquid interface will not cause much alteration of the flow field in Taylor flow (Bretherton, 1961; Ratulowski and Chang, 1990). Since our experiments were mainly carried out at Ca on the order of 10^{-2} (see Figs. 5(a) and (b)), the influence of Marangoni effect on pressure drop of Taylor flow is expected to be somewhat insignificant here.

To interpret the experimental data in both microchannels more reasonably, an extra item was added to the function ξ in the Kreutzer correlation in the following way:

$$\xi = a\left(\frac{L_S}{d_h}\right)^{-1}\left(\frac{\rho_L d_h \sigma}{\mu_L^2}\right)^{1/3} + b\left(\frac{L_S}{d_h Re_{\text{slug}}}\right)^{m} \tag{23}$$

The second item in the right side of Eq. (23) was designed to reflect the strong influence of inner recirculation in very short liquid slugs that is not revealed in the simulation of Kreutzer et al. (2005b). In view of the dominance of developing flow conditions in such short liquid slugs, it was assumed that the added item might be simply expressed as a power function of $L_S/d_h Re_{\text{slug}}$, which was analogous to the analysis method previously adopted in the study on the apparent friction factor under hydrodynamically developing flow for non-circular ducts (Muzychka and Yovanovich, 1998; Shah and London, 1978). Then, by a least square regression analysis of the current data, the empirical constants b and m associated with this item were obtained and a new expression for f_{slug} was found as

$$f_{\text{slug}} = \frac{56.9}{Re_{\text{slug}}}\left[1 + 0.07\left(\frac{L_S}{d_h}\right)^{-1}\left(\frac{\rho_L d_h \sigma}{\mu_L^2}\right)^{1/3} + 5.5\times 10^{-5}\left(\frac{L_S}{d_h Re_{\text{slug}}}\right)^{-1.6}\right] \tag{24}$$

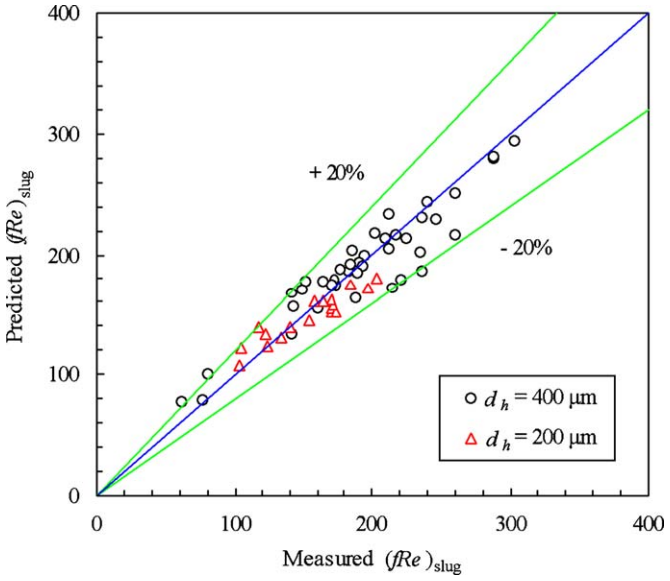

Fig. 10. Comparison between the measured $(fRe)_{\text{slug}}$ values and predictions of Eq. (24) in square microchannels.

Fig. 10 compares the measured $(fRe)_{\text{slug}}$ values with the predictions of this expression, where relatively small standard deviations of 11.1% and 9.4% were achieved for the two microchannels with $d_h = 400$ and 200 μm, respectively. From Eq. (24), it seems that the inner recirculation is strengthened especially for shorter liquid slugs and higher values of Re_{slug}. Moreover, it is also shown that the added new item in the bracket, $5.5\times 10^{-5}(L_S/d_h Re_{\text{slug}})^{-1.6}$, can be omitted if the liquid slug is not very short. For example, under the condition of $L_S/d_h = 3$ and $Re_{\text{slug}} = 200$, this item only takes a value of about 0.05, which is much smaller than the sum of the other items in the bracket. In this case, this equation is essentially the same as Eq. (15) proposed by Kreutzer et al. (2005b). Thus it is believed that Eq. (24) can be used to describe pressure drop data of air–water Taylor flow in square microchannels within a wide range of operational conditions. However, since only experiments of air–water flow are dealt with here, the extrapolation of this equation to other fluid pairs should be taken with caution. In the latter case, pressure drop characteristics of Taylor flow with short liquid slugs still awaits further simulation work as well as experimental validation.

3.3. Mass transfer characteristics

In order to predict the performance of gas–liquid reactions as well as solid catalyzed gas–liquid reactions conducted under Taylor flow in microchannels, it is essential to gain a thorough understanding of mass transfer details inside this flow pattern.

It is noteworthy that considerable attention has been paid to mass transfer studies in Taylor flow through millimeter-sized capillaries during the past years (Berčič and Pintar, 1997; Heiszwolf et al., 2001; Irandoust et al., 1992; Kreutzer et al., 2001; van Baten and Krishna, 2004; Vandu et al., 2005). These studies have made it clear that the overall liquid side volumetric mass transfer coefficient $k_L a$ (the

product of liquid side mass transfer coefficient k_L and interfacial area a) in Taylor flow is highly dependent on the local flow details therein. Among them, a representative experimental work was carried out by Berčič and Pintar (1997) who found that the measured k_La during methane–water Taylor flow in circular capillaries of 1.5, 2.5 and 3.1 mm diameters could be estimated by the following empirical correlation:

$$k_La = \frac{0.111(j_G + j_L)^{1.19}}{((1-\varepsilon_G)(L_B+L_S))^{0.57}} \tag{25}$$

Since it is reasonable to assume that $(1-\varepsilon_G)(L_B+L_S) \approx L_S$ if the liquid slug is not very short, Eq. (25) suggests that k_La is largely dependent on the liquid slug length rather than that of the bubble. Thus Berčič and Pintar (1997) concluded that the contribution of mass transfer from the bubble caps to the liquid slug was dominant in their experiments. Later van Baten and Krishna (2004) performed a CFD simulation of mass transfer in Taylor flow through circular capillaries of 1.5, 2 and 3 mm diameters, where Taylor bubble was assumed to consist of two hemispherical caps and a cylindrical body. They considered that Eq. (25) might be only capable of predicting k_La at long contact times between the liquid film and the bubble since many experimental data of Berčič and Pintar (1997) were obtained with very long bubbles and liquid slugs. For comparatively short film contact times (corresponding to large values of bubble velocity and small unit cell lengths), van Baten and Krishna (2004) found that the obtained k_La values in the simulation deviated significantly from the predictions of Eq. (25). Instead, k_La values could be well represented by their proposed mass transfer model in which separated contributions of mass transfer from the body of the bubble to the surrounding liquid film and mass transfer from the two bubble caps to the liquid slug were both considered. That is,

$$k_La = k_{L,\,\mathrm{film}}a_{\mathrm{film}} + k_{L,\,\mathrm{cap}}a_{\mathrm{cap}} \tag{26}$$

where liquid side mass transfer coefficients in the liquid film and the liquid slug, i.e., $k_{L,\,\mathrm{film}}$ and $k_{L,\,\mathrm{cap}}$, were derived based on the penetration theory (Higbie, 1935) as

$$k_{L,\,\mathrm{film}} = 2\sqrt{\frac{D}{\pi t_{\mathrm{film}}}} \tag{27}$$

$$k_{L,\,\mathrm{cap}} = 2\frac{\sqrt{2}}{\pi}\sqrt{\frac{DU_B}{d_h}} \tag{28}$$

And interfacial areas for the liquid film and two hemispherical caps, i.e., a_{film} and a_{cap}, can be calculated as

$$a_{\mathrm{film}} = \frac{\pi d_B L_{\mathrm{film}}}{\frac{\pi}{4}d_h^2(L_B+L_S)} \approx \frac{4(L_B-d_h)}{d_h(L_B+L_S)} \tag{29}$$

$$a_{\mathrm{cap}} = \frac{\pi d_B^2}{\frac{\pi}{4}d_h^2(L_B+L_S)} \approx \frac{4}{L_B+L_S} \tag{30}$$

In the above equations, L_{film} is the length of the liquid film surrounding the bubble, and t_{film} refers to the contact time between the liquid film and the bubble, which can be evaluated from

$$t_{\mathrm{film}} = \frac{L_{\mathrm{film}}}{U_B} \approx \frac{L_B-d_h}{U_B} \tag{31}$$

Then the mass transfer model of van Baten and Krishna (2004) can be further rewritten as

$$k_La = \frac{2}{\sqrt{\pi}}\sqrt{\frac{DU_B}{(L_B-d_h)}}\frac{4(L_B-d_h)}{d_h(L_B+L_S)} + 2\frac{\sqrt{2}}{\pi}\sqrt{\frac{DU_B}{d_h}}\frac{4}{(L_B+L_S)} \tag{32}$$

Recently Vandu et al. (2005) have experimentally verified the applicability of Eq. (32) for mass transfer under air–water Taylor flow in 1, 2 and 3 mm diameter capillaries of circular and square cross-sections by further assuming that the major contribution to mass transfer was $k_{L,\,\mathrm{film}}a_{\mathrm{film}}$.

In this study, we have performed mass transfer measurements during air–water Taylor flow in SMC I with $d_h = 400\,\mu\mathrm{m}$. For the physical absorption of oxygen from air into water, gas side mass transfer resistance is negligible. Then, by assuming a macroscopic plug flow behavior for the liquid phase, k_La in the main microchannel can be expressed as

$$k_La = \frac{j_L}{\Delta L}\ln\left(\frac{C^* - C_{O_2,\,0}}{C^* - C_{O_2,\,1}}\right) \tag{33}$$

Here, $C_{O_2,\,0}$ is the concentration of dissolved oxygen in the water entering the main microchannel of SMC I, which was thought to be the same as that measured in the liquid tank. To derive the concentration of dissolved oxygen in the water leaving the main microchannel, $C_{O_2,\,1}$, reference experiments were conducted using SMC II under the same volumetric flow rates of gas and liquid as those for SMC I. Based on the assumptions that hydrodynamic conditions in the outlet zones of both contactors were nearly the same, average liquid side volumetric mass transfer coefficients therein were thought to be equal as well (Yue et al., 2007). Therefore, there should be

$$\frac{C^* - C_{O_2,\,1}}{C^* - C_{O_2,\,2}} = \frac{C^* - C'_{O_2,\,0}}{C^* - C_{O_2,\,3}} \tag{34}$$

In this equation, $C'_{O_2,\,0}$ denotes the concentration of dissolved oxygen in the water entering SMC II while $C_{O_2,\,2}$ and $C_{O_2,\,3}$ are concentrations of dissolved oxygen measured in the water collected in the phase separator during experiments with SMCs I and II, respectively. From Eqs. (33) and (34), k_La in the microchannel can be finally obtained from the experiments as

$$k_La = \frac{j_L}{\Delta L}\ln\left(\frac{(C^* - C_{O_2,\,3})(C^* - C_{O_2,\,0})}{(C^* - C_{O_2,\,2})(C^* - C'_{O_2,\,0})}\right) \tag{35}$$

To check whether the above-mentioned two representative mass transfer correlations (i.e., Eqs. (25) and (32)) are further applicable in the current microchannel, the measured k_La data are compared to the predictions of these equations in Fig. 11. It should be noted that the gas hold up data in Eq. (25) are given by

$$\varepsilon_G = \frac{j_G}{U_B} \tag{36}$$

It is obvious in Fig. 11 that neither of the two equations can give a reasonable description of the present data. Both equations tend to yield higher k_La values than the measurements, where more significant deviation was found in the predictions of Eq. (32) proposed by van Baten and Krishna (2004). It is known that both equations were proposed for circular capillaries. Then the direct application of these equations to the present square microchannel will certainly cause some degree of certainty in their predictions due to somewhat large difference of the liquid film profile as well as the shape of the front and rear bubble caps herein from that in circular capillaries (Vandu et al., 2005). But in our opinion, this uncertainty is not the main cause responsible for the deviation observed in Fig. 11. As mentioned before, the two equations were thought to be valid under certain mass transfer circumstances. Eq. (25) might be useful in predicting k_La at large film contact times where the transfer of gas into the liquid slug is dominant whereas Eq. (32) is recommended at short film contact times where the transfer of gas into the liquid film and the liquid slug are both important. van Baten and Krishna (2004) suggested $Fo < 0.1$ as a criterion for short film contact times,

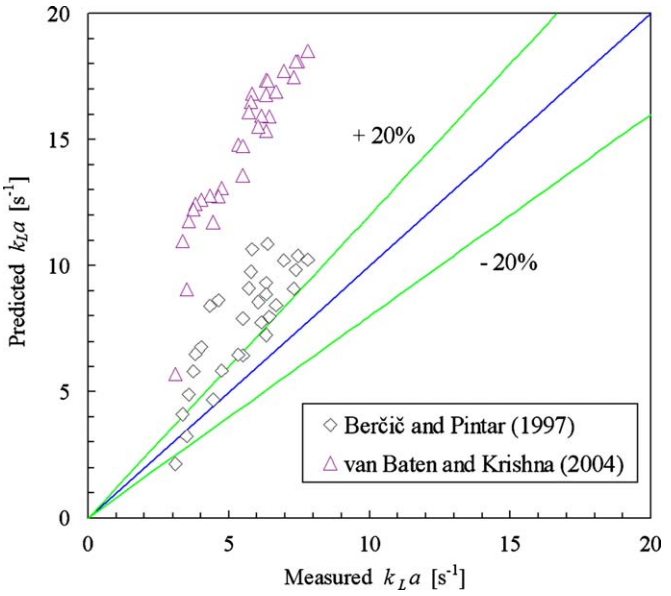

Fig. 11. Comparison of the measured k_La values with predictions of the existing mass transfer correlations in the square microchannel with $d_h = 400\,\mu m$.

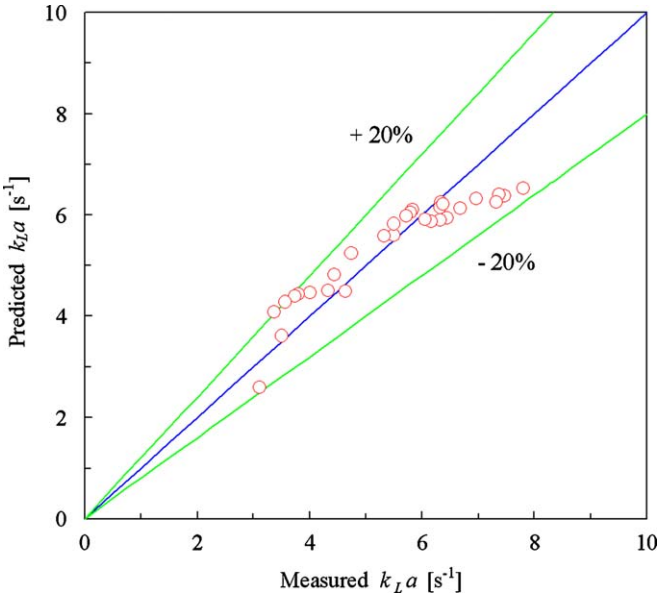

Fig. 12. Comparison of the measured k_La values with predictions of Eq. (38) in the square microchannel with $d_h = 400\,\mu m$.

where Fourier number Fo is defined as $Fo = Dt_{film}/\delta^2_{film}$. In the current mass transfer experiments, a rough estimation revealed that Fo was on the order of 0.01. Therefore, at first sight one may consider that Eq. (32) is more appropriate for describing the current data and the poor predicting performance of Eq. (25) can be easily understood since this equation loses its validity here. However, the even worse predicting performance of Eq. (32) implies that there must be some other factors that may lead to its inapplicability.

In fact, another important assumption for the validity of Eq. (32) is the complete mixing between the liquid film and the liquid slug. In Taylor flow, the liquid film is alternatively exposed to Taylor bubble and the liquid slug. The mass transfer process between the liquid film and the liquid slug (i.e., the transfer of dissolved gas) take places predominantly by diffusion without the presence of strong convective mixing (Thulasidas et al., 1999). If a complete mixing is always achieved between the above two regions, a well-mixed liquid phase in each unit cell along the microchannel is warranted. Then, it is easy to show that the overall k_La value can be expressed as the sum of $k_{L,\,film}a_{film}$ and $k_{L,\,cap}a_{cap}$ according to the penetration theory (Higbie, 1935). In the majority of CFD simulations conducted by van Baten and Krishna (2004), the liquid slug was much longer than the bubble (see Table 1 in their paper for further information). The mixing of the liquid film with such long liquid slug is more likely to be complete (Kreutzer et al., 2005a; Thiers et al., 1971), which would explain why their simulations agreed well with the predictions of Eq. (32). However, it is observed in our mass transfer experiments that length of liquid slugs produced in the current microchannel was normally very short (e.g., $< 3d_h$, see also Fig. 9(a)). This implies that the mixing between the liquid film and the liquid slug should be rather incomplete in our experiments. Under this circumstance, the dissolved gas in the liquid film cannot be effectively transferred into the liquid slug, which subsequently leads to a significant decrease in the local absorption rate in the liquid film along the microchannel as compared to the complete mixing case. Thus it has been observed in Fig. 11 that the experimental k_La values are much lower than the model predictions of van Baten and Krishna (2004).

To interpret mass transfer data obtained in the present microchannel with $d_h = 400\,\mu m$, it is assumed that k_La therein can be expressed approximately in the following form:

$$k_La = \frac{c}{d_h}\left(\frac{DU_B}{d_h}\right)^{0.5}\left(\frac{L_B}{d_h}\right)^{n}\left(\frac{L_B+L_S}{d_h}\right)^{p} \tag{37}$$

The empirical constants c, n and p were determined to be about 2, 0.3, −0.8, respectively, on the basis of a regression analysis of the experimental data. Finally, we can obtain the following empirical correlation for the estimation of k_La in this microchannel

$$k_La = \frac{2}{d_h}\left(\frac{DU_B}{L_B+L_S}\right)^{0.5}\left(\frac{L_B}{L_B+L_S}\right)^{0.3} \tag{38}$$

Fig. 12 shows the comparison of the experimental k_La values with those predicted by this correlation. The standard deviation was found to be as low as 10.8%, implying a good fitting performance of this correlation (the ranges of parameters investigated are: $0.4\,m/s < U_B < 2\,m/s$, $1.4 < L_B/d_h < 6.3$, $1 < L_S/d_h < 3.2$, $d_h = 400\,\mu m$). It is seen from Eq. (38) that the measured k_La shows great dependence on the bubble velocity and the length of the unit cell. Especially, an increase in k_La is anticipated when the bubble velocity increases or the liquid slug length is reduced, which follows exactly the same trend as that suggested by Eq. (32). Furthermore, Eq. (38) implies that the film contribution to mass transfer is important or at least not negligible in our experiments since the measured k_La is strongly influenced by the length of the whole unit cell instead of the liquid slug length alone. But it should be pointed out here that the current data are still not sufficient. To further elucidate the macroscopic mass transfer results observed in our experiments, the microscopic interplay between the liquid film and slug mass transfer contributions inside each unit cell along the microchannel should be made clear. Therefore, a detailed numerical analysis is currently underway.

4. Conclusions

In this paper, flow and mass transfer issues in air–water Taylor flow through two square microchannels with hydraulic diameters of 400 and 200 μm have been investigated experimentally.

Experimental data on Taylor bubble velocity, pressure drop as well as liquid side volumetric mass transfer coefficient have been presented and analyzed. Based on the results of this study, the following conclusions can be drawn:

(1) Taylor bubble in square microchannels was found to move slightly faster than the liquid slug due to the existence of a nearly stagnant film surrounding the bubble body. The experimental bubble velocity results can be well interpreted based upon an approximate measurement of the liquid film profile in microchannels, where it was shown that the velocity ratio between Taylor bubble and the liquid slug further increased with increasing *Ca* primarily as a result of the thickening of the liquid film in the corner of the microchannel cross-section.

(2) Two-phase frictional pressure drop of Taylor flow through microchannels should be expressed as the sum of the frictional losses in the liquid slug, in the liquid film and pressure drop over the bubble caps. The experimental pressure drop data of air–water Taylor flow in the current two microchannels were found to agree well with those predicted by the correlation of Kreutzer et al. (2005b) only at large liquid slug length. Nevertheless, a significant underestimation in the prediction has been observed when the liquid slug length is short than about 1.5 times hydraulic diameter of the microchannel, which can be explained by the inadequacy of this correlation to describe the excess pressure drop caused by the strong inner circulation in such short liquid slugs. An appropriate modification has been made to this correlation in order to improve its applicability in microchannels.

(3) The available correlations for the estimation of liquid side volumetric mass transfer coefficient in Taylor flow through capillaries proposed by Berčič and Pintar (1997) and van Baten and Krishna (2004) show large deviation from our experimental mass transfer data in the square microchannel with $d_h = 400\,\mu m$. An accompanying analysis has revealed that due to rather short liquid slugs produced in this microchannel, mass transfer experiments were mainly operated under the condition of short film contact time and rather poor mixing between the liquid film and the liquid slug, which was not in accordance with mass transfer assumptions associated with the above two correlations. A new empirical correlation has therefore been proposed to describe the experimental results with reasonable predicting accuracy.

Notation

a	interfacial area, m^2/m^3
A	cross-sectional area, m^2
b	empirical constant in Eq. (23)
c	empirical constant in Eq. (37)
C	laminar friction constant
Ca	capillary number defined by $(=\mu_L U_B/\sigma)$, dimensionless
C_{O_2}	molar concentration of O_2 in the water, mol/m^3
$C'_{O_2,0}$	molar concentration of O_2 in the water entering SMC II, mol/m^3
C^*	physical solubility of O_2 in the water, mol/m^3
d_B	diameter of hemispherical bubble caps, m
d_h	hydraulic diameter, m
D	liquid phase diffusivity, m^2/s
f	friction factor
Fo	Fourier number defined by $(=Dt_{film}/\delta_{film}^2)$, dimensionless
G	mass flux defined by $(=j_G\rho_G + j_L\rho_L)$, $kg/(m^2\,s)$
j	superficial velocity, m/s
k_L	liquid side mass transfer coefficient, m/s
k_La	liquid side volumetric mass transfer coefficient, s^{-1}
L_B	length of Taylor bubble, m
L_{film}	length of the liquid film, m
L_S	length of the liquid slug, m
ΔL	length of the main microchannel, m
m	empirical constant in Eq. (23)
n	empirical constant in Eq. (37)
p	empirical constant in Eq. (37)
$P_{in,\,SMC\,I}$	inlet pressure in the gas feeding line during experiments with SMC I, Pa
$P_{in,\,SMC\,II}$	inlet pressure in the gas feeding line during experiments with SMC II, Pa
ΔP	pressure drop, Pa
ΔP_A	two-phase acceleration pressure drop, Pa
ΔP_F	two-phase frictional pressure drop, Pa
ΔP_T	two-phase total pressure drop, Pa
Q	volumetric flow rate, m^3/s
$\underline{r}$	circular arc radius of liquid in the diagonal plane, m
r_b	radius of the bubble cylindrical body, m
Re_{slug}	liquid slug Reynolds number defined by $(=d_h U_{slug}\rho_L/\mu_L)$, dimensionless
t_{film}	contact time between the liquid film and Taylor bubble, s
U	mean velocity, m/s
W_{film}	width of the liquid film in the axial plane, m
x	gas mass fraction

Greek letters

α	coefficient in Eq. (16)
β	phase volumetric fraction
δ_{film}	thickness of the liquid film surrounding the body of the bubble, m
ε	hold up
μ	viscosity, Pa s
ζ	extra pressure function defined in Eq. (15)
ρ	density, kg/m^3
σ	surface tension, N/m

Subscripts

0	microchannel entrance
1	microchannel outlet
2	in the phase separator during experiments with SMC I
3	in the phase separator during experiments with SMC II
B	Taylor bubble
cap	bubble cap
film	liquid film
G	gas phase
L	liquid phase
mc	microchannel
slug	liquid slug
TP	two-phase mixture
uc	a unit cell of Taylor flow

Acknowledgments

This work was supported by France ANR (Agence Nationale de la Recherche) within the “programme non thématique 2005” (no. NT05-3_41570), National Natural Science Foundation of China (nos. 20490208 and 20676129), and Ministry of Science and Technology of China (nos. 2007AA030206 and 2009CB219903). We also wish to thank Dr. Rhaphaël Boichot and Mr. Raymond Sedano for assistance with the experiments.

References

Abdallah, R., Magnico, P., Fumey, B., de Bellefon, C., 2006. CFD and kinetic methods for mass transfer determination in a mesh microreactor. A.I.Ch.E. Journal 52, 2230–2237.

Angeli, P., Gavriilidis, A., 2008. Hydrodynamics of Taylor flow in small channels: a review. Proceedings of the Institution of Mechanical Engineers, Part C: Journal of Mechanical Engineering Science 222, 737–751.

Aussillous, P., Quéré, D., 2000. Quick deposition of a fluid on the wall of a tube. Physics of Fluids 12, 2367–2371.

Berčič, G., Pintar, A., 1997. The role of gas bubbles and liquid slug lengths on mass transport in the Taylor flow through capillaries. Chemical Engineering Science 52, 3709–3719.

Bretherton, F.P., 1961. The motion of long bubbles in tubes. Journal of Fluid Mechanics 10, 166–188.

Chambers, R.D., Holling, D., Spink, R.C.H., Sandford, G., 2001. Elemental fluorine Part 13. Gas–liquid thin film microreactors for selective direct fluorination. Lab on a Chip 1, 132–137.

Chen, G., Yue, J., Yuan, Q., 2008. Gas–liquid microreaction technology: recent advances and future challenges. Chinese Journal of Chemical Engineering 16, 663–669.

Chen, J.D., 1986. Measuring the film thickness surrounding a bubble inside a capillary. Journal of Colloid and Interface Science 109, 341–349.

Chung, P.M.-Y., Kawaji, M., 2004. The effect of channel diameter on adiabatic two-phase flow characteristics in microchannels. International Journal of Multiphase Flow 30, 735–761.

Cox, B.G., 1964. An experimental investigation of the streamlines in viscous fluid expelled from a tube. Journal of Fluid Mechanics 20, 193–200.

de Mas, N., Günther, A., Schmidt, M.A., Jensen, K.F., 2003. Microfabricated multiphase reactors for the selective direct fluorination of aromatics. Industrial and Engineering Chemical Research 42, 698–710.

Dulkler, A.E., Hubbard, M.G., 1975. A model for gas–liquid slug flow in horizontal and near horizontal tubes. Industrial and Engineering Chemistry Research 14, 337–347.

Ehrfeld, W., Hessel, V., Löwe, H., 2000. Microreactors: New Technology for Modern Chemistry. Wiley-VCH, Weinheim.

Fairbrother, F., Stubbs, A.E., 1935. Studies in electro-endosmosis. Part VI. The "bubble-tube" method of measurement. Journal of the Chemical Society 1, 527–529.

Fries, D.M., Trachsel, F., von Rohr, P.R., 2008. Segmented gas–liquid flow characterization in rectangular microchannels. International Journal of Multiphase Flow 34, 1108–1118.

Fuerstman, M.J., Lai, A., Thurlow, M.E., Shevkoplyas, S.S., Stone, H.A., Whitesides, G.M., 2007. The pressure drop along rectangular microchannels containing bubbles. Lab on a Chip 7, 1479–1489.

Garimella, S., Killion, J.D., Coleman, J.W., 2002. An experimentally validated model for two-phase pressure drop in the intermittent flow regime for circular microchannels. Journal of Fluids Engineering 124, 205–214.

Griffith, P., Wallis, G.B., 1961. Two-phase slug flow. Journal of Heat Transfer 83, 307–320.

Günther, A., Khan, S.A., Thalmann, M., Trachsel, F., Jensen, K.F., 2004. Transport and reaction in microscale segmented gas–liquid flow. Lab on a Chip 4, 278–286.

Heiszwolf, J.J., Kreutzer, M.T., van den Eijnden, M.G., Kapteijn, F., Moulijn, J.A., 2001. Gas–liquid mass transfer of aqueous Taylor flow in monoliths. Catalysis Today 69, 51–55.

Hessel, V., Hardt, S., Löwe, H., 2004. Chemical Micro Process Engineering: Fundamentals, Modelling and Reactions. Wiley-VCH, Weinheim.

Hessel, V., Löwe, H., Müller, A., Kolb, G., 2005a. Chemical Micro Process Engineering: Processing and Plants. Wiley-VCH, Weinheim.

Hessel, V., Angeli, P., Gavriilidis, A., Löwe, H., 2005b. Gas–liquid and gas–liquid–solid microstructured reactors: contacting principles and applications. Industrial and Engineering Chemistry Research 44, 9750–9769.

Higbie, R., 1935. The rate of absorption of a pure gas into a still liquid during short periods of exposure. Transactions of the A.I.Ch.E. 31, 365–389.

Inoue, T., Schmidt, M.A., Jensen, K.F., 2007. Microfabricated multiphase reactors for the direct synthesis of hydrogen peroxide from hydrogen and oxygen. Industrial and Engineering Chemistry Research 46, 1153–1160.

Irandoust, S., Ertle, S., Andersson, B., 1992. Gas–liquid mass-transfer in Taylor flow through a capillary. The Canadian Journal of Chemical Engineering 70, 115–119.

Jähnisch, K., Baerns, M., Hessel, V., Ehrfeld, W., Haverkamp, V., Löwe, H., Wille, Ch., Guber, A., 2000. Direct fluorination of toluene using elemental fluorine in gas/liquid microreactors. Journal of Fluorine Chemistry 105, 117–128.

Kobayashi, J., Mori, Y., Okamoto, K., Akiyama, R., Ueno, M., Kitamori, T., Kobayashi, S., 2004. A microfluidic device for conducting gas–liquid–solid hydrogenation reactions. Science 304, 1305–1308.

Kolb, W.B., Cerro, R.L., 1991. Coating the inside of a capillary of square cross-section. Chemical Engineering Science 46, 2181–2195.

Kreutzer, M.T., Du, D., Heiszwolf, J.J., Kapteijn, F., Moulijn, J.A., 2001. Mass transfer characteristics of three-phase monolith reactors. Chemical Engineering Science 56, 6015–6023.

Kreutzer, M.T., Kapteijn, F., Moulijn, J.A., Heiszwolf, J.J., 2005a. Multiphase monolith reactors: chemical reaction engineering of segmented flow in microchannels. Chemical Engineering Science 60, 5895–5916.

Kreutzer, M.T., Kapteijn, F., Moulijn, J.A., Kleijn, C.R., Heiszwolf, J.J., 2005b. Inertial and interfacial effects on pressure drop of Taylor flow in capillaries. A.I.Ch.E. Journal 51, 2428–2440.

Leclerc, A., Alamé, M., Schweich, D., Pouteau, P., Delattre, C., de Bellefon, C., 2008. Gas–liquid selective oxidations with oxygen under explosive conditions in a micro-structured reactor. Lab on a Chip 8, 814–817.

Liu, H., Vandu, C.O., Krishna, R., 2005. Hydrodynamics of Taylor flow in vertical capillaries: flow regimes, bubble rise velocity, liquid slug length, and pressure drop. Industrial and Engineering Chemistry Research 44, 4884–4897.

Losey, M.W., Schmidt, M.A., Jensen, K.F., 2001. Microfabricated multiphase packed-bed reactors: characterization of mass transfer and reactions. Industrial and Engineering Chemistry Research 40, 2555–2562.

Muzychka, Y.S., Yovanovich, M.M., 1998. Modeling friction factors in non-circular ducts for developing laminar flow. In: Proceedings of the Second AIAA Theoretical Fluid Mechanics Meeting, AIAA Paper 98–2492, Albuquerque, NM, 15–18 June 1998.

Ratulowski, J., Chang, H.-C., 1990. Marangoni effects of trace impurities on the motion of long gas bubbles in capillaries. Journal of Fluid Mechanics 210, 303–328.

Schulze, G., Schlünder, E.U., 1985. Physical absorption of single gas bubbles in degassed and preloaded water. Chemical Engineering and Processing 19, 27–37.

Serizawa, P.A., Feng, Z.P., Kawara, Z., 2002. Two-phase flow in microchannels. Experimental Thermal and Fluid Science 26, 703–714.

Shah, R.K., London, A.L., 1978. Laminar Flow Forced Convection in Ducts. Academic Press, New York.

Taylor, G.I., 1961. Deposition of a viscous fluid on the wall of a tube. Journal of Fluid Mechanics 10, 161–165.

TeGrotenhuis, W.E., Cameron, R.J., Viswanathan, V.V., Wegeng, R.S. Solvent extraction and gas absorption using microchannel contactors. In: Proceedings of the Third International Conference on Microreaction Technology, Springer, Berlin, 2000, pp. 541–549.

Thiers, R.E., Reed, A.H., Delander, K., 1971. Origin of the lag phase of continuous-flow analysis curves. Clinical Chemistry 17, 42–48.

Thulasidas, T.C., Abraham, M.A., Cerro, R.L., 1995. Bubble-train flow in capillaries of circular and square cross section. Chemical Engineering Science 50, 183–199.

Thulasidas, T.C., Abraham, M.A., Cerro, R.L., 1997. Flow patterns in liquid slugs during bubble-train flow inside capillaries. Chemical Engineering Science 52, 2947–2962.

Thulasidas, T.C., Abraham, M.A., Cerro, R.L., 1999. Dispersion during bubble-train flow in capillaries. Chemical Engineering Science 54, 61–76.

Trachsel, F., Günther, A., Khan, S., Jensen, K.F., 2005. Measurement of residence time distribution in microfluidic systems. Chemical Engineering Science 60, 5729–5737.

Triplett, K.A., Ghiaasiaan, S.M., Abdel-Khalik, S.I., Sadowski, D.L., 1999. Gas–liquid two-phase flow in microchannels. Part I: two-phase flow patterns. International Journal of Multiphase Flow 25, 377–394.

van Baten, J.M., Krishna, R., 2004. CFD simulations of mass transfer from Taylor bubbles rising in circular capillaries. Chemical Engineering Science 59, 2535–2545.

Vandu, C.O., Liu, H., Krishna, R., 2005. Mass transfer from Taylor bubbles rising in single capillaries. Chemical Engineering Science 60, 6430–6437.

Vasconcelos, J.M.T., Orvalho, S.P., Alves, S.S., 2002. Gas–liquid mass transfer to single bubbles: effect of surface contamination. A.I.Ch.E. Journal 48, 1145–1154.

Wallis, G.B., 1969. One Dimensional Two-Phase Flow. McGraw-Hill, New York, USA.

Wang, X., Nie, Y., Jasmine, L.C.L., Jaenicke, S., 2007. Evaluation of multiphase microreactors for the direct formation of hydrogen peroxide. Applied Catalysis A: General 317, 258–265.

Warnier, M.J.F., Rebrov, E.V., de Croon, M.H.J.M., Hessel, V., Schouten, J.C., 2008. Gas hold-up and liquid film thickness in Taylor flow in rectangular microchannels. Chemical Engineering Journal 135 (Suppl. 1), S153–S158.

Wong, H., Radke, C.J., Morris, S., 1995a. The motion of long bubbles in polygonal capillaries. Part 1. Thin films. Journal of Fluid Mechanics 292, 71–94.

Wong, H., Radke, C.J., Morris, S., 1995b. The motion of long bubbles in polygonal capillaries. Part 2. Drag, fluid pressure and fluid-flow. Journal of Fluid Mechanics 292, 95–110.

Yeong, K.K., Gavriilidis, A., Zapf, R., Hessel, V., 2003. Catalyst preparation and deactivation issues for nitrobenzene hydrogenation in a microstructured falling film reactor. Catalysis Today 81, 641–651.

Yue, J., Chen, G., Yuan, Q., Luo, L., Gonthier, Y., 2007. Hydrodynamics and mass transfer characteristics in gas–liquid flow through a rectangular microchannel. Chemical Engineering Science 62, 2096–2108.

Yue, J., Luo, L., Gonthier, Y., Chen, G., Yuan, Q., 2008. An experimental investigation of gas–liquid two-phase flow in single microchannel contactors. Chemical Engineering Science 63, 4189–4202.

Zhao, T.S., Bi, Q.C., 2001. Pressure drop characteristics of gas–liquid two-phase flow in vertical miniature triangular channels. International Journal of Heat and Mass Transfer 44, 2523–2534.